EJN fens EUROPEAN JOURNAL OF NEUROSCIENCE

European Journal of Neuroscience, Vol. 35, pp. 1753–1760, 2012 doi:10.1111/j.1460-9568.2012.08094.x

NEUROSYSTEMS

Enhancement of neural representation capacity by modular architecture in networks of cortical neurons

Ofri Levy, Noam E. Ziv and Shimon Marom
Faculty of Medicine and Network Biology Laboratories, Technion, Haifa, Israel

Keywords: classification, modularity, multi-electrode array, neural network, representation scheme

Abstract

Biological networks are ubiquitously modular, a feature that is believed to be essential for the enhancement of their functional capacities. Here, we have used a simple modular *in vitro* design to examine the possibility that modularity enhances network functionality in the context of input representation. We cultured networks of cortical neurons obtained from newborn rats *in vitro* on substrate-integrated multi-electrode arrays, forcing the network to develop two well-defined modules of neural populations that are coupled by a narrow canal. We measured the neural activity, and examined the capacity of each module to individually classify (i.e. represent) spatially distinct electrical stimuli and propagate input-specific activity features to their downstream coupled counterpart. We show that, although each of the coupled modules maintains its autonomous functionality, a significant enhancement of representational capacity is achieved when the system is observed as a whole. We interpret our results in terms of a relative decorrelation effect imposed by weak coupling between modules.

Introduction

Brain architecture is inherently modular, being composed of local networks that are embedded in networks of networks, which are sparsely connected to each other (Mountcastle, 1997; Rockland, 1998; Schreiner *et al.*, 2000; Erdi & Kiss, 2001; Ferrarini *et al.*, 2009; Meunier *et al.*, 2010). Extensive electrophysiological and imaging analyses *in vivo* suggest that brain modularity is a key determinant of our cognitive capacities, having impacts on both dynamic and functional aspects of neural activity (Hubel & Wiesel, 1977; Sporns *et al.*, 2000; Derdikman *et al.*, 2003; Diamond *et al.*, 2003; Op de Beeck *et al.*, 2008; Kumar *et al.*, 2010; Pan *et al.*, 2010; Boucsein *et al.*, 2011). Although very informative, these *in vivo* analyses do not allow for well-controlled manipulation of structural and temporal constraints on the dynamics and functions of modular networks, limiting the generalizability of findings. In recent years, *in vitro* technologies supported by advanced substrate patterning methods have made it possible to force neural networks to develop a range of predefined modular structures. While far from being 'real' brains, these *in vitro* designs have proved useful in studies aimed at the characterization of activity dynamics in modular networks. In particular, such studies have demonstrated that modular networks exhibit a large repertoire of reoccurring activity patterns (Raichman & Ben-Jacob, 2008), as well as the dependency of activity propagation on the density of projections that couple two adjacent modules (Maeda *et al.*, 1995; Feinerman *et al.*, 2005, 2008; Yvon *et al.*, 2005; Berdondini *et al.*, 2006; Rutten *et al.*, 2007; Baruchi *et al.*, 2008; Dworak & Wheeler, 2009; Massobrio *et al.*, 2009; Shein *et al.*, 2009; Wheeler & Brewer, 2010; Pan *et al.*, 2011).

Correspondence: O. Levy, as above.
E-mail: ofril@tx.technion.ac.il

Received 2 August 2011, revised 14 February 2012, accepted 27 February 2012

Here, we took advantage of the *in vitro* modular system in order to investigate a functional aspect of modularity. As pointed out by others (Tononi & Edelman, 1998; Zeki & Bartels, 1998; Hartwell *et al.*, 1999), functionality in modular systems depends on a tradeoff between differentiation and integration; that is, a tradeoff between the requirement to maintain the functional separation and autonomy of each module in itself, and allowing for functional integration of the modular system as a whole, by which enhancement of functional capacities is achieved. We have approached the above tradeoff in the context of a minimal system that is composed of two coupled neural modules, focusing on aspects of a key function that neural networks are believed to realize, that is, representation.

We coupled two large-scale networks of cortical neurons *in vitro* through a narrow connecting path, and recorded evoked spiking activity by using multi-electrode array (MEA) technology. We examined the capacity of each network (module) to individually distinguish between input sources and propagate input-specific activity features to its 'downstream' coupled counterpart. We demonstrate that each of the modules has the capacity to be active, and to process and represent its own input sources in an independent manner, in accordance with the differentiation aspect of modularity. We further demonstrate an instantiation of the integrative aspect of modularity by showing that a downstream module can enhance the representational capacity of the system by amplifying the differences between response features of the upstream (stimulated) module.

Materials and methods

Culture preparation and modular design

The experimental design was approved by the Inspection Committee on the Constitution of the Animal Experimentation at the Technion.

Cortical neurons were obtained from newborn rats (Sprague–Dawley) within 24 h after birth, with standard procedures (Marom & Shahaf, 2002). Prior to dissection, rats were deeply anesthetized with CO_2. The brains were removed, and the cortex tissue was digested enzymatically with 0.05% trypsin solution in phosphate-buffered saline (PBS) (Dulbecco's PBS) free of calcium and magnesium, supplemented with 20 mM gucose, at 37 °C. Enzyme treatment was terminated with heat-inactivated horse serum (Biological Industries, Beit-Haemek, Israel), and cells were then mechanically dissociated. Dissociated neurons were suspended in minimal essential medium, supplemented with heat-inactivated horse serum (5%), glutamine (0.5 mM), glucose (20 mM), and gentamicin (20 μM). A few hours before cells were plated on the MEA [MultiChannelSystems (MCS), Reutlingen, Germany], the MEA surface was coated with laminin (Sigma, St. Louis, MO, USA), and the modular structure (see below) was installed. The cells were then plated in each module at a similar density ($\sim$ 500 cells/mm^2). One day later, after cells had adhered to the MEA, 1.5 mL of growth medium was added. The preparations were allowed to develop and mature over a time period of 15–21 day *in vitro* prior to the experiments. Variability in the number of culture days in this range had no effect on the observed results. The cultures were maintained in an atmosphere of 37 °C, 5% CO_2 and 95% air within the incubator, as well as during the electrophysiological measurements.

The modular structure was prepared from polydimethylsiloxane (PDMS) (Sylgard 184; Dow-Corning, Midland, MI, USA), with photoresist and chemical etching techniques, following Dworak & Wheeler (2009), and slightly modified for our needs; see also Korin *et al.* (2007). The structure consisted of two wells (modules); the area of each module was 4 mm^2, and the two modules were connected by a 200 × 800-μm canal. The PDMS structure was aligned onto the MEA with a drop of 70% ethanol, and placed on a hot plate at 40 °C for 2 h to allow reversible binding to the surface. MEAs of 60 Ti/Au/TiN electrodes, 30 μm in diameter each, were used. The array design consisted of four clusters (zones) of 13 electrodes, symmetrically located (two in each module) and separated from each other by 1 mm. Electrodes within each of these four zones were spaced 200 μm from each other (Fig. 1A).

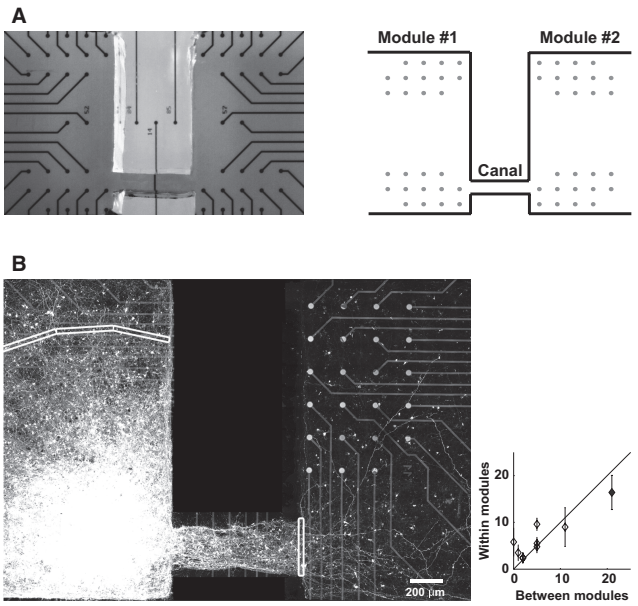

FIG. 1. Modular preparation. (A) A PDMS barrier with a narrow canal is attached to the MEA to separate neural populations ('modules'). An image of the modular setup is shown on the left, and a schematic drawing on the right. Four remote zones of electrodes (two within each module) are shown. (B) Extensions projecting from the lower area of module 1 are traced by selective neuronal labeling with the fluorescent lipophilic dye DiD, to illustrate the restriction of projections crossing to a coupled module (see Materials and methods). Note that the electrode layout in the thin MEAs used for these imaging experiments is different from the one used for electrophysiological measurements. The right panel compares the number of extensions crossing the exit of the canal (*x*-axis, counted in eight labeled networks) with the number of extensions crossing segments of the same size as the canal width, located within the labeled module at a similar distance from the labeling locus (*y*-axis). Segments in which extensions were counted are marked by rectangles in the labeled network image. Measurements from the particular network shown on the left are indicated by a black diamond.

Fluorescent labeling of fibers

The fluorescent dye DiD (1,1-dioctadecyl-3,3,3,3-tetramethylindodicarbocyanine, 4-chlorobenzenesulfonate; Invitrogen, Carlsbad, CA, USA) was applied by microinjection, according to Ziv & Smith (1996), in a sterile environment. Following staining, the cultures were gently washed to remove excess dye, and maintained at 37 °C in an atmosphere of 5% CO_2 and 95% air for 3 days to allow diffusion of the dye. Scanning fluorescence and DIC images were acquired with a custom-designed confocal laser scanning microscope based on a Zeiss Axiovert 200, using a × 40 1.3-NA Fluar objective, as described previously (Tsuriel *et al.*, 2006). DiD was excited by means of a 632-nm helium neon laser, and fluorescence emissions were read with the use of 650-nm-long-pass edge filters (Semrock, New York, USA). In these imaging experiments, special thin glass MEAs were used, which are different from those used for electrophysiological measurements. Data were collected sequentially from multiple predefined sites across the entire modular network with custom software, and stitched according to Rankov *et al.* (2005). Non-linear contrast enhancement (gamma adjustment) was used to emphasize the labeling.

Measurements and stimulation

A commercial 60-channel amplifier (B-MEA-1060; MCS) with frequency limits of 150–5000 Hz and a gain of × 1024 was used. In experiments involving stimulation, current or voltage stimuli (200-μs biphasic 10–50 μA or monophasic 600–800 mV) were generated with a dedicated stimulus generator (MCS). In the context of this study, no difference was observed in the behavior of neurons under current or voltage stimulation. The stimuli were delivered once every 15–20 s, to minimize adaptation of the network response. Data were digitized with either two parallel 5200a/526 A/D boards (Microstar Laboratories, Bellevue, WA, USA) after further amplification by MCPPlus variable gain filter amplifiers (Alpha Omega, Nazareth, Israel), or the USB-ME256 system (MCS). Each channel was sampled at a frequency of 24 000 samples/s, and prepared for analysis with the ALPHAMAP interface (Alpha Omega), or MC-RACK software (MCS) and an open source MATLAB toolbox (Egert *et al.*, 2002). Thresholds for spike detection (× 8 RMS units; typically in the range of 10–20 μV) were defined separately for each of the recording channels prior to the beginning of the experiment. Analyses were performed in a MATLAB environment (MathWorks, Natwick, MA, USA). Where synaptic blockade is indicated in the text, a solution of 20 μM amino-5-phosphonovaleric acid, 10 μM 6-cyano-7-nitroquinoxaline-2,3-dione, and 5 μM bicuculline methiodide was used.

Data analysis

Spontaneous network spikes (NSs) were detected on the basis of activity threshold, following an earlier study (Eytan & Marom, 2006).

The data around each NS detection time (± 250 ms) were extracted. Population spike count histograms (PSCHs) were constructed for each module by registering the total spike count in an NS, binned at 1-ms time resolution. Mean values ± standard deviations are shown, unless mentioned otherwise. Statistical significance was determined with a two-sided paired Student's *t*-test.

For classification analyses, two spatially distinct electrical stimuli were applied to one module, and the module responses were analysed. The first 15 ms following stimulation were removed from evoked responses (as elaborated in Results), and PSCHs were binned at 5-ms time resolution. Several constraints were imposed in order to avoid trivialization of classification efficacy evaluation: Only 'broadly tuned electrodes' active in at least 70% of the NSs were considered, while similar amount of recording units in both modules were maintained. In addition, only fully developed NSs, in which the total firing rate in each module exceeded the averaged firing rate across NSs, were considered. For unsupervised classification, all of the responses of each module were compared with each other for similarity. Distance (dissimilarity) between each pair of PSCH vectors was computed by city-block metric distance (also known as 'Manhattan' or 'L1' distance), following normalization to the higher total spike count within 150 ms post-stimulus of the response pair. Distances between vectors of the total spike count (within 150 ms post-stimulus) of each neuron within each module, and between vectors of the time delay from the stimulus onset to the first spike evoked by each neuron, were also computed by city-block distance, following normalization of each pair of vectors to the higher mean value. The contrast measure was obtained by comparing the mean distance between responses to the same input source with the mean distance between responses to different input sources [subtraction of the mean distance between responses to the same input source from the mean distance between responses to different input sources, normalized by the sum of the means; see Beggs & Plenz (2004)]. Supervised classification analysis was performed with the support vector machine (SVM) algorithm with a Gaussian radial-based function kernel, as elaborated in earlier studies (Shahaf *et al.*, 2008; Kermany *et al.*, 2010). The SVM was applied to training sets of PSCH vectors, and the resulting classifiers were then validated with test set vectors. MCSVM1.0 (webee.technion.ac.il/people/koby), a C code package for multi-class SVM, was applied (Crammer & Singer, 2001). Kernel parameter and confidence intervals were set with a five-fold cross-validation procedure.

Results

Spontaneous activity in modular networks

We cultured modular networks of cortical neurons *in vitro* on substrate-integrated MEAs. This was achieved by attaching to the substrate a physical barrier, which forces the network to develop two well-defined modules of homogeneously distributed neural populations with similar cell densities, coupled by a narrow canal (see Materials and methods and Fig. 1A). This structural constraint allows for extensive connectivity between neurons within each module, and restricted (i.e. weak) connectivity between modules. In Fig. 1B, selective neuronal labeling with the fluorescent lipophilic dye DiD, which diffuses retrogradely and anterogradely along the dendrites and axons (Agmon *et al.*, 1995; Ziv & Smith, 1996; Gan *et al.*, 2000; Kobbert *et al.*, 2000), demonstrates the restriction imposed by the canal on the connecting fibers crossing from one module to its coupled counterpart. Neurons at the lower area of one module were labeled, and neurites projecting from the labeled area across the canal to the coupled module, and to remote areas within the labeled module, were traced. An image of one labeled network is shown in the left panel of Fig. 1B. The right panel shows measurements from eight labeled networks. The number of neurites crossing the exit of the canal (5.7 ± 6.5 extensions) was similar to the number of neurites crossing each one of multiple segments (depicted in the image) of the same size as the canal width, located within the labeled module at a similar distance as the canal from the labeling locus (6.6 ± 4.8 extensions). Thus, a higher number of connecting fibers projected within a module than between modules.

The spontaneous spiking activity of the modular networks is largely composed of synchronous spiking events that are initiated within one of the modules, and, in most cases (91% ± 11%, n = 19 370 events, seven networks), propagate with a short time delay into the coupled module. Henceforth, following an earlier study (Eytan & Marom, 2006), we use the term NS to denote an individual synchronous event. Raster plots of single NSs from one network are shown in Fig. 2A.

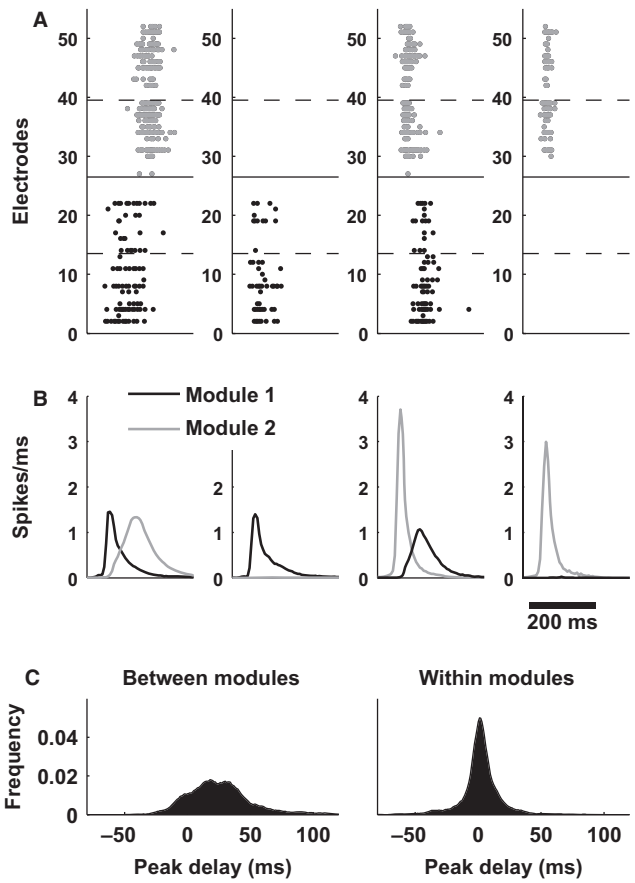

FIG. 2. Dynamics of spontaneous activity. (A) Raster plots showing typical NSs from one modular network. Solid horizontal lines separate neurons belonging to different modules (depicted gray and black); dashed lines separate recordings at remote zones within each module. NSs are shown according to their module of origin: examples are shown in which they propagate between the coupled modules (first and third columns), or stay within their module of origin (second and fourth columns). (B) PSCHs of each module (gray and black) from the same network shown in A, binned at 5-ms time resolution, and averaged across NSs (a total of 5800 NSs, one network). The different columns of B match the columns of A, representing subsets of NSs classified according to their module of origin and whether they propagate between the coupled modules. (C) Distribution of time delays between activity peaks of coupled modules (left), and over similar distance within modules (right) from seven networks.

Figure 2B shows PSCHs (the total spike count binned at 1-ms time resolution, as described in Materials and methods) of the activity within each module, averaged across all NSs of the same network shown in Fig. 2A. Figure 2A and B shows the NSs according to their module of origin (modules are depicted gray and black), and exemplifies cases in which activity propagated from one module to the other or remained within the module of origin.

Where NSs propagated from one module to the other, the average delay between the peak of activity at the module of origin and at the downstream module was 25.98 ± 26.61 ms (averaged across all NSs in seven networks). These delays spanned a wider range than the rapid propagation within a module, over a similar distance (1.9 ± 16.3 ms; Fig. 2C). Such a comparison between propagation of the activity within and between modules was made possible by taking advantage of the MEA layout, in which four zones of electrodes are symmetrically located–two within each module (Fig. 1A). In Fig. 2A, recordings from remote zones within each module are separated by a dashed line. As can be seen in Fig. 2A, the population activity at the different zones within each module was highly synchronized, and showed similar activity profiles–as if they belonged to one entity.

At later stages of the NS, following the delayed recruitment of activity at the downstream succeeding module, synchronization of the activity was observed among the coupled modules as well. This synchronicity was most apparent at secondary activity peaks in the module of origin, which occurred in close temporal proximity to the primary peak of the downstream module (Fig. 3A). The prevalence of the short time delays between these activity peaks (mean time delays of 7.6 ± 29.1 ms, seven networks) is shown in Fig. 3B. This late intermodular synchronization suggests that, subsequent to the delayed recruitment of the downstream module, activity reverberates across the coupled networks with mutual activation.

Evoked activity in modular networks

When a pulse of electrical stimulation was delivered to a given module, the neural population of that module responded in two phases, in agreement with previous reports (Jimbo *et al.*, 2000; Kermany *et al.*, 2010): an initial short phase, dominated by the activity of a directly stimulated subset of neurons, followed by a slower wave of activity resulting from synaptically mediated propagation throughout the module. Traces of the first component (direct response) were detectable in the coupled (non-stimulated) module, although these, in themselves, were insufficient to initiate the second (slow) phase in that coupled module. This was demonstrated by application of synaptic blockers to one module but not to its coupled counterpart (by applying a solution of 20 μM amino-5-phosphonovaleric acid, 10 μM 6-cyano-7-nitroquinoxaline-2,3-dione and 5 μM bicuculline directly to the cells of that module). Stimulation of the unblocked module resulted in a full NS at that module, which did not propagate to the synaptically blocked module–confirming the selectivity of the blockade for only one module. Stimulation of the blocked module, however, elicited only the direct responses in both modules, whereas, before application of synaptic blockers, similar stimulation elicited full NSs that propagated to both modules (Fig. 4). Thus, to induce an NS in the downstream module, a full-blown NS must be evoked in the stimulated module.

Synaptically mediated evoked activity propagated from the stimulated module to the downstream coupled module with a delay that was similar to that of spontaneously evoked NSs (averaged activity peak delays of 26.26 ± 26.23 ms, n = 48 000 evoked NSs in nine networks). Likewise, the overall slow-phase time–amplitude envelope of evoked NSs was similar in nature to that of spontaneously generated NSs. As in spontaneous NSs, not all evoked responses propagated to the coupled module (85% ± 23%, nine networks); this is in contrast to the consistent spread of activity within a module. The longer propagation delays and the lower probability of propagation between modules than within modules are indicative of the capacity of each module to act separately from its counterpart.

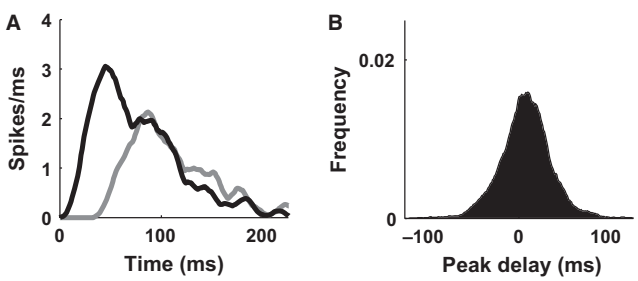

FIG. 3. Late synchronization of activity between modules. (A) PSCHs of coupled modules (black and gray) from one NS, demonstrating late synchronization of the population activity in the coupled modules. A secondary activity peak is observed at the module of origin in close temporal proximity to the primary peak of the succeeding module. (B) Distribution of time delays between the primary activity peak of the downstream module and a secondary peak at the module of origin, indicating short delays.

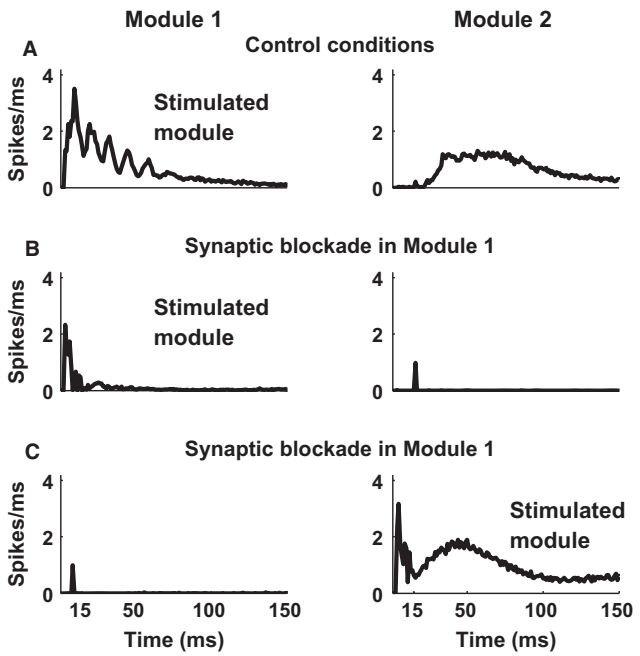

FIG. 4. An experiment demonstrating propagation of evoked responses between coupled modules. (A) Electrical stimulation was applied to module 1 (left column). Averaged PSCHs of the responses (n = 200 evoked NSs in one network) at the stimulated module are shown in the left column, and the responses at the downstream coupled module (module 2) are shown in the right column. Note the delayed propagation of activity to the coupled module. (B) Responses of each module to the same stimulation source in module 1 (n = 120 evoked NSs), following selective blockade of synaptic activity in module 1. Only the immediate phase of response to the stimulation is present in this stimulated module (left column), as well as in the downstream coupled module (right column). (C) Synaptic blockade in module 1 does not impact on the capacity of stimulation in module 2 to evoke a full response in module 2, verifying the confinement of the blockers to module 1. Under such conditions, the response of module 2 to stimulation does not propagate to the coupled (synaptically blocked) module 1 (left column). Similar results were obtained with different stimulation sites at the same network.

Functional benefits of modular organization; enhanced representation capacity

We turn now to the impacts of modular organization on the efficacy of the network in representing input sources. Although the very concept of neural representation is far from being understood, the functional aspect of it can be operationally viewed as the capacity to classify distinct inputs on the basis of neuronal activity features ('representation schemes', 'neural codes') (e.g. deCharms & Zador, 2000; Luna *et al.*, 2005; Averbeck *et al.*, 2006). The choice of the representational function in the present context relies on recent results that have demonstrated the capacity of neuronal networks *in vitro* to reliably classify spatial and temporal input features using both rate-based and time-based schemes (Shahaf *et al.*, 2008; Kermany *et al.*, 2010).

We applied two spatially distinct electrical stimuli (through different stimulating electrodes) to one module, and evaluated the capacity to distinguish between these stimuli by using the temporal profile of evoked population activity (PSCHs), both within the stimulated module and in its coupled module. We focus on the representation capacity of synaptically mediated activity, beyond the (rather trivial) capacity to classify input sources on the basis of the direct response phase. The latter is mostly confined to the first 15 ms following stimulation, as can be learned from synaptically blocked preparations (92.1% ± 9.8% of evoked neural spikes that occurred within 30 ms post-stimulus were confined to the initial 15 ms, in 860 evoked responses to seven stimulation sources, at two synaptically blocked networks), and from previous reports (Jimbo *et al.*, 2000; Marom & Shahaf, 2002; Bakkum *et al.*, 2008; Kermany *et al.*, 2010); therefore, the first 15 ms of activity were removed from the analysed data. Figure 5 shows an example of averaged PSCHs in response to two stimulation sources applied to one of the modules. In this example, the two stimuli were applied to the lower zone of module 1 (depicted), and the responses of each recording zone in each module were measured. Propagation along similar distances between modules (across the lower zones of the neighboring modules) and within the same module (across the lower and upper zones of the same module) were examined. Upon propagation of the activity onto the downstream coupled module, responses to the different stimuli became more distinct. In contrast, within a module over a similar distance, the temporal envelope of the responses displayed similar activity profiles, and differences between the responses to the two stimulation sources did not increase.

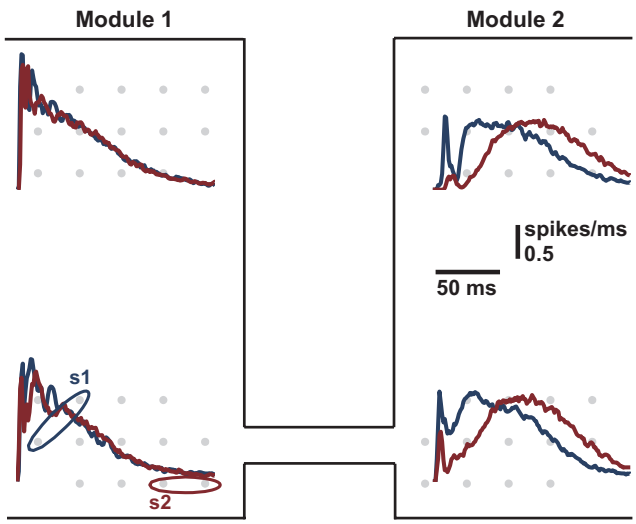

FIG. 5. Representation of spatially distinct inputs by coupled modules. An example of the responses of a network to two spatially distinct input sources, delivered to one module, is shown. The stimulating electrodes are indicated by different colors in a schematic diagram of the modular structure. In this example, the two stimuli were applied to the lower zone of module 1. Responses of neural populations in the different zones within the stimulated and the downstream coupled module (n = 476 evoked responses) are presented as averaged PSCHs in each zone, colored according to the identity of the input source. Note the enhanced separation of responses in module 2, as compared with the stimulated module 1. No apparent effect of distance within a module is observed.

To directly assess the representation efficacy of each module in all 35 experiments (i.e. different input source pairs) conducted on nine networks, their capacity to distinguish between input sources was estimated by the use of an unsupervised classification algorithm. All responses in each module were compared with each other for the level of similarity, a city-block metric being used to assess the distance (i.e. 'dissimilarity') between each pair of responses (see Materials and methods). A contrast measure was then applied to evaluate classification capacity, by comparing the averaged distances between the responses within and between input sources (Beggs & Plenz, 2004) (see Materials and methods). Behavioral studies (Thorpe & Fabre-Thorpe, 2001; Vanrullen, 2007) and physiological studies *in vivo* (Slovin *et al.*, 2002; Harris *et al.*, 2003) and *in vitro* (Eytan & Marom, 2006; Kermany *et al.*, 2010) indicate that stimulus selective activity and its feedforward transfer to a downstream module occur within several tens of milliseconds (see Marom, 2010); therefore, classification was evaluated with the initial 50 ms of the response PSCHs. The stimulated module's stimulus classification efficacy was similar whether or not NSs propagated downstream to the coupled module (P = 0.154, paired t-test); this is an indication of the capacity of a stimulated module to function independently of its coupled counterpart. Figure 6 compares the classification capacities of the stimulated and the downstream modules, in cases where the evoked activity did propagate downstream. Distance matrices calculated from one exemplar experiment are shown in Fig. 6A for each module. Each matrix shows the distances between all pairs of responses in that module. Distances are shown in grayscale and sorted according to stimulus identity. Marked contrast between the responses to the different input sources, indicating high classification capacity, was observed at the downstream module's distance matrix (module 2, right panel). Results from all 35 experiments are shown in Fig. 6B; statistically significant higher contrast values (i.e. better classifications, $P < 0.0001$, paired t-test) were observed at the downstream module (module 2). Enhancement of classification at the coupled module was also observed by evaluation of the entire PSCH length (P = 0.0079). In addition, the enhanced classification was not limited to the rising phase, as significantly higher contrast values at the downstream modules were observed by evaluation of time windows centered around the peaks of the evoked activity (P = 0.0013).

In 29 of the experiments, conducted on eight networks, the pairs of stimuli were delivered to the lower zone of one of the modules, and PSCHs were evaluated for each of the modular network's zones (in a similar manner as in the example shown in Fig. 5A). The stimulation site pairs were chosen arbitrarily from the point of view of their position relative to each of the adjacent neighboring zones, with different stimulating electrode positions being examined. Classification capacity was significantly enhanced when activity propagated through the narrow canal between the lower zones of the coupled modules ($P < 0.0001$), but not by propagation along a similar distance to the upper zone of the stimulated module (P = 0.71) (mean contrast values and 95% confidence intervals computed with Student's t-test were 0.041, 0.02–0.062, 0.043, 0.021–0.065 and 0.137, 0.096–0.178 in the stimulated zone, upper zone of the same module, and lower

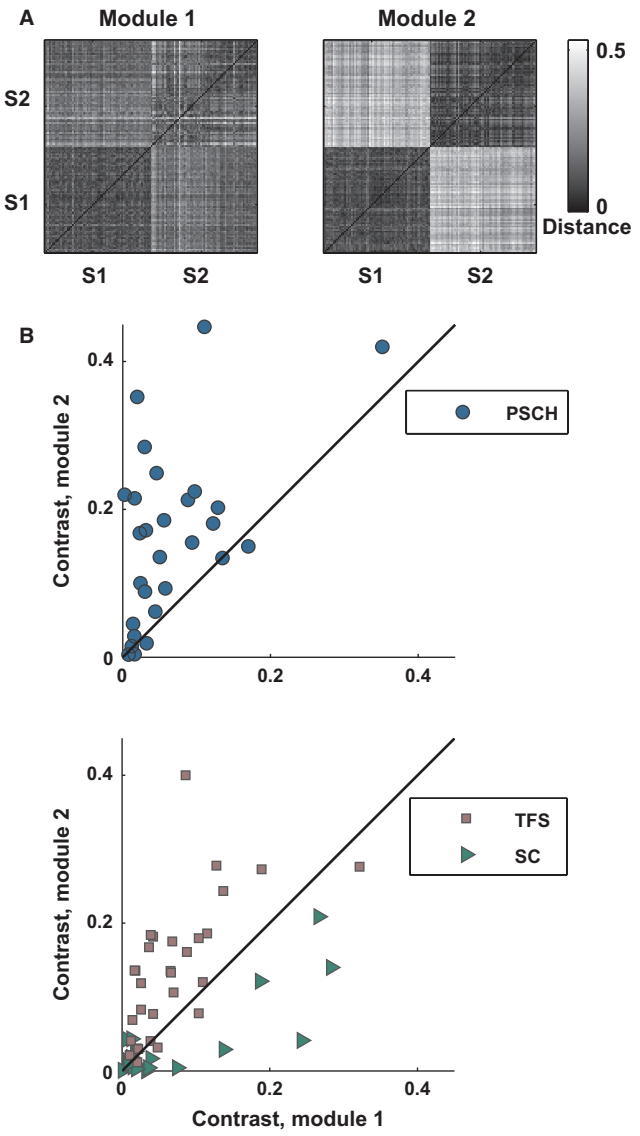

FIG. 6. Unsupervised two-source classification task. (A) Classification with the initial 50 ms of the modules PSCHs in one network as an example. Distance matrices showing the distances between all pairs of responses of each module in comparison with each other (n = 136 evoked responses). Distances (computed by city-block distance; see Materials and methods) are shown in grayscale and sorted by stimulus identity. The distance matrix of the stimulated module is shown in the left panel, and that of its coupled counterpart is shown in the right panel. Separation between responses to different stimuli (observed as higher contrast) is prominent at the downstream coupled module. (B) A contrast measure (see Materials and Methods) is used, reflecting the level of similarity among responses to the same input source relative to different sources – indicating classification efficacy. For each network, the contrast measure for the downstream module (y-axis, module 2) is plotted against that of the stimulated module (x-axis, module 1); n = 35 classification task experiments conducted on nine networks. The upper panel shows contrast measures obtained with the initial 50 ms of the PSCHs. Significantly higher classification capacity is observed at the downstream coupled module ($P < 0.0001$). The lower panel shows contrast measures applied on other representational schemes. Squares indicate classification by the time delays from stimulation to the first spike evoked by each neuron [time to first spike (TFS)]; here, too, classification is significantly enhanced at the downstream module ($P < 0.0001$). Triangles show evaluation of the total spike counts (SCs; in a 150-ms time window post-stimulus) of individual neurons; significantly lower classification at the downstream module is observed (P = 0.004). The reduced classification is insignificant when classification is based on spike counts in shorter time windows.

zone of the coupled module, respectively). Significantly enhanced classification at the lower zone of the coupled module relative to the upper zone of the stimulated module was observed as well ($P < 0.0001$). The position of stimulation sites relative to each of the neighboring zones did not affect the direction of the results. As can be seen in Fig. 5A, the response to stimulation s2, which was closer to module 2, produced a longer delay in the coupled module than s1. The responses of the coupled module to the closer stimulus showed longer delays in 16 of the 35 experiments, and shorter delays in the rest of the experiments. This indicates that the observed enhancement of the differences between responses to distinct input sources is not affected by propagation along different distances but by propagation through the narrow canal.

Interestingly, the enhanced representational capacity of a downstream module was not unaffected by the nature of the representation scheme used (i.e. 'neural code'): the results of unsupervised classification based on two other representation schemes (see Materials and methods) are shown in the lower panel of Fig. 6B. When vectors of the time delays from stimulus onset to the first spike evoked by each neuron were considered (squares), classification in the downstream module was enhanced as well ($P < 0.0001$). However, classification based on the total spike counts of individual neurons (in a 150-ms time window post-stimulus, triangles) degraded when activity propagated out of the stimulated module (reduced classification, P = 0.004).

Enhancement of classification capacity by PSCHs in downstream coupled modules was also demonstrated by use of a non-parametric classification technique, a general purpose supervised classifier Support Vector Machine (SVM) with an adaptive Gaussian kernel (Ben-Hur *et al.*, 2008; Shahaf *et al.*, 2008; Kermany *et al.*, 2010) (see Materials and methods for details). The SVM was trained to classify the different input sources at different time windows following stimulation. A separation hyper-plane was constructed on the basis of labeled examples of the data, and a lower bound on classification capacity was estimated by its performance on a test dataset. Figure 7 compares the classification capacities of the stimulated and the downstream modules. Classification capacity was quite good in both modules, being highest at the earlier stages of the synaptically mediated responses, and decaying at later times. Classification was significantly better at the downstream coupled module (P = 0.0028 and P = 0.0039 at time windows of 16–50 ms and 51–75 ms post-

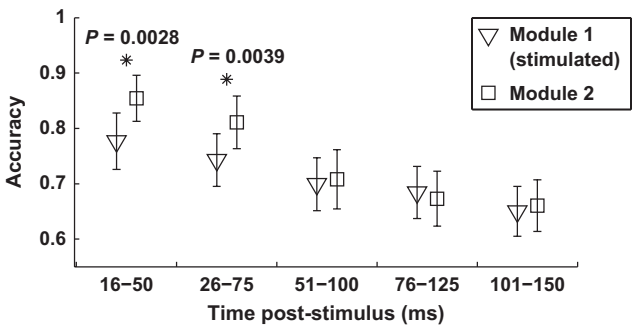

FIG. 7. Supervised classification analysis. Two-source classification capacity of the response PSCHs of the stimulated module and its coupled module, computed with a supervised classifier, SVM (n = 35 input sources pairs, in nine networks). The classification capacities at different time windows following the stimulus were evaluated separately. Mean values and 95% confidence intervals computed with Student's t-test are shown (n = 35 input source pairs, in nine networks). Asterisks indicate significant differences between the classification capacities of the coupled modules ($P < 0.05$). At early times following stimulation, the downstream coupled module classification is significantly higher.

stimulus, respectively), an advantage that vanished at the late stages of the responses.

Discussion

A key advantage of a modular system, relative to a homogeneous system of a similar size, is the capacity of the former to enhance its functionality by lumping the different modules together (functional integration), while–at the same time–maintaining the autonomy of each individual module (functional differentiation). Here, we demonstrated an instantiation of this advantage in a simple modular *in vitro* design of cultured cortical neurons, in the context of input representation – a most basic function exercised by the brain. We observed functional differentiation in the form of an autonomous capacity of each module in itself to classify (represent) spatial input sources, separately from its coupled module. This classification capacity of an individual module is similar to previously reported results (Shahaf *et al.*, 2008; Kermany *et al.*, 2010), and is independent of whether or not activity spreads to the coupled module. Functional integration was manifested as a significant enhancement of classification capacity when the activity evoked in one module propagated to the downstream coupled module. The observed enhancement of representation capacity is enabled by the modular structure itself, which imposes sparse connectivity between modules, and does not occur over a similar distance within an extensively connected homogeneous network. Furthermore, we showed that the weak coupling between the two modules imposed a 20–30-ms delay in the propagation of input selective activity, within the range of delays observed *in vivo* (Thorpe & Fabre-Thorpe, 2001; Slovin *et al.*, 2002). The enhanced capacity of a downstream module to classify an upstream input source degrades within $\sim$ 100 ms of the application of the stimulus. The main result–enhanced representational capacity in the downstream module–is sensitive to the representation scheme ('neural code') used: modularity enhances classification when the temporal features of the population activity are considered, but not when classification relies on spike counts of individual neurons.

We offer our interpretation of an enhanced population representation scheme in terms of a relative decorrelation effect that a narrow canal of connectivity imposes on the propagated activity. When activity propagates within one module through the many extensively connected neurons involved, small differences between responses to different stimulation sources are dissipated by interference. In contrast, the activity forced to propagate into a downstream module through the narrow canal is relatively immune to the effect. This relative decorrelation, imposed by the canal, effectively enhances the classification contrast.

Acknowledgements

The authors thank Vladimir and Elleonora Lyakhov for invaluable technical assistance, Daniel Dagan, Asaf Gal, Elad Schneidman and Avner Wallach for useful comments and suggestions, Shy Shoham's group for technical assistance in imaging experiments, and Bruce Wheeler's laboratory for their help in first steps of patterning over MEA. The research leading to these results has received funding from the European Union Seventh Framework Program FP7 under grant agreement 269 459, and was also supported by a grant of the Ministry of Science and Technology of the State of Israel and MATERA grant agreement 3-7878.

Abbreviations

MCS, MultiChannelSystems; MEA, multi-electrode array; NS, network spike; PBS, phosphate-buffered saline; PDMS, polydimethylsiloxane; PSCH, population spike count histogram; SVM, support vector machine.

References

Agmon, A., Yang, L.T., Jones, E.G. & O'Dowd, D.K. (1995) Topological precision in the thalamic projection to neonatal mouse barrel cortex. *J. Neurosci.*., **15**, 549–561.

Averbeck, B.B., Latham, P.E. & Pouget, A. (2006) Neural correlations, population coding and computation. *Nat. Rev.*, **7**, 358–366.

Bakkum, D.J., Chao, Z.C. & Potter, S.M. (2008) Long-term activity-dependent plasticity of action potential propagation delay and amplitude in cortical networks. *PLoS One*, **3**, e2088.

Baruchi, I., Volman, V., Raichman, N., Shein, M. & Ben-Jacob, E. (2008) The emergence and properties of mutual synchronization in *in vitro* coupled cortical networks. *Eur. J. Neurosci.*, **28**, 1825–1835.

Beggs, J.M. & Plenz, D. (2004) Neuronal avalanches are diverse and precise activity patterns that are stable for many hours in cortical slice cultures. *J. Neurosci.*, **24**, 5216–5229.

Ben-Hur, A., Ong, C.S., Sonnenburg, S., Scholkopf, B. & Ratsch, G. (2008) Support vector machines and kernels for computational biology. *PLoS Comput. Biol.*, **4**, e1000173.

Berdondini, L., Chiappalone, M., van der Wal, P.D., Imfeld, K., de Rooij, N.F., Koudelka-Hep, M., Tedesco, M., Martinoia, S., van Pelt, J., Le Masson, G. & Garenne, A. (2006) A microelectrode array (MEA) integrated with clustering structures for investigating *in vitro* neurodynamics in confined interconnected sub-populations of neurons. *Sensors Actuators B*, **114**, 530–541.

Boucsein, C., Nawrot, M.P., Schnepel, P. & Aertsen, A. (2011) Beyond the cortical column: abundance and physiology of horizontal connections imply a strong role for inputs from the surround. *Front. Neurosci.*, **5**, 1–13.

deCharms, R.C. & Zador, A. (2000) Neural representation and the cortical code. *Annu. Rev. Neurosci.*, **23**, 613–647.

Crammer, K. & Singer, Y. (2001) On the algorithmic implementation of multiclass kernel-based vector machines. *J. Machine Learn. Res.*, **2**, 265–292.

Derdikman, D., Hildesheim, R., Ahissar, E., Arieli, A. & Grinvald, A. (2003) Imaging spatiotemporal dynamics of surround inhibition in the barrels somatosensory cortex. *J. Neurosci.*, **23**, 3100–3105.

Diamond, M.E., Petersen, R.S., Harris, J.A. & Panzeri, S. (2003) Investigations into the organization of information in sensory cortex. *J. Physiol. Paris*, **97**, 529–536.

Dworak, B.J. & Wheeler, B.C. (2009) Novel MEA platform with PDMS microtunnels enables the detection of action potential propagation from isolated axons in culture. *Lab Chip*, **9**, 404–410.

Egert, U., Knott, T., Schwarz, C., Nawrot, M., Brandt, A., Rotter, S. & Diesmann, M. (2002) MEA-Tools: an open source toolbox for the analysis of multi-electrode data with MATLAB. *J. Neurosci. Methods*, **117**, 33–42.

Erdi, P. & Kiss, T. (2001) The complexity of the brain: structural, functional, and dynamic modules. In Wermter, S., Austin, J. & Willshaw, D. (Eds), *Emergent Neural Computational Architectures Based on Neuroscience*. Springer, Berlin, Heidelberg, pp. 203–211.

Eytan, D. & Marom, S. (2006) Dynamics and effective topology underlying synchronization in networks of cortical neurons. *J. Neurosci.*, **26**, 8465–8476.

Feinerman, O., Segal, M. & Moses, E. (2005) Signal propagation along unidimensional neuronal networks. *J. Neurophysiol.*, **94**, 3406–3416.

Feinerman, O., Rotem, A. & Moses, E. (2008) Reliable neuronal logic devices from patterned hippocampal cultures. *Nat. Phys.*, **4**, 967–973.

Ferrarini, L., Veer, I.M., Baerends, E., van Tol, M.J., Renken, R.J., van der Wee, N.J., Veltman, D.J., Aleman, A., Zitman, F.G., Penninx, B.W., van Buchem, M.A., Reiber, J.H., Rombouts, S.A. & Milles, J. (2009) Hierarchical functional modularity in the resting-state human brain. *Hum. Brain Mapp.*, **30**, 2220–2231.

Gan, W.B., Grutzendler, J., Wong, W.T., Wong, R.O. & Lichtman, J.W. (2000) Multicolor 'DiOlistic' labeling of the nervous system using lipophilic dye combinations. *Neuron*, **27**, 219–225.

Harris, K.D., Csicsvari, J., Hirase, H., Dragoi, G. & Buzsaki, G. (2003) Organization of cell assemblies in the hippocampus. *Nature*, **424**, 552–556.

Hartwell, L.H., Hopfield, J.J., Leibler, S. & Murray, A.W. (1999) From molecular to modular cell biology. *Nature*, **402**, C47–52.

Hubel, D.H. & Wiesel, T.N. (1977) Ferrier lecture. Functional architecture of macaque monkey visual cortex. *Proc. R. Soc. Lond. B*, **198**, 1–59.

Jimbo, Y., Kawana, A., Parodi, P. & Torre, V. (2000) The dynamics of a neuronal culture of dissociated cortical neurons of neonatal rats. *Biol. Cybern.*, **83**, 1–20.

Kermany, E., Gal, A., Lyakhov, V., Meir, R., Marom, S. & Eytan, D. (2010) Tradeoffs and constraints on neural representation in networks of cortical neurons. *J. Neurosci.*, **30**, 9588–9596.

Kobbert, C., Apps, R., Bechmann, I., Lanciego, J.L., Mey, J. & Thanos, S. (2000) Current concepts in neuroanatomical tracing. *Prog. Neurobiol.*, **62**, 327–351.

Korin, N., Bransky, A., Dinnar, U. & Levenberg, S. (2007) A parametric study of human fibroblasts culture in a microchannel bioreactor. *Lab Chip*, **7**, 611–617.

Kumar, A., Rotter, S. & Aertsen, A. (2010) Spiking activity propagation in neuronal networks: reconciling different perspectives on neural coding. *Nat. Rev.*, **11**, 615–627.

Luna, R., Hernandez, A., Brody, C.D. & Romo, R. (2005) Neural codes for perceptual discrimination in primary somatosensory cortex. *Nat. Neurosci.*, **8**, 1210–1219.

Maeda, E., Robinson, H.P. & Kawana, A. (1995) The mechanisms of generation and propagation of synchronized bursting in developing networks of cortical neurons. *J. Neurosci.*, **15**, 6834–6845.

Marom, S. (2010) Neural timescales or lack thereof. *Prog. Neurobiol.*, **90**, 16–28.

Marom, S. & Shahaf, G. (2002) Development, learning and memory in large random networks of cortical neurons: lessons beyond anatomy. *Q. Rev. Biophys.*, **35**, 63–87.

Massobrio, P., Tedesco, M., Giachello, C., Ghirardi, M., Fiumara, F. & Martinoia, S. (2009) Helix neuronal ensembles with controlled cell type composition and placement develop functional polysynaptic circuits on micro-electrode arrays. *Neurosci. Lett.*, **467**, 121–126.

Meunier, D., Lambiotte, R. & Bullmore, E.T. (2010) Modular and hierarchically modular organization of brain networks. *Front. Neurosci.*, **4**, 1–11.

Mountcastle, V.B. (1997) The columnar organization of the neocortex. *Brain*, **120**(Pt 4), 701–722.

Op de Beeck, H.P., Haushofer, J. & Kanwisher, N.G. (2008) Interpreting fMRI data: maps, modules and dimensions. *Nat. Rev.*, **9**, 123–135.

Pan, R.K., Chatterjee, N. & Sinha, S. (2010) Mesoscopic organization reveals the constraints governing Caenorhabditis elegans nervous system. *PLoS One*, **5**, 1–15.

Pan, L., Alagapan, S., Franca, E., Brewer, G.J. & Wheeler, B.C. (2011) Propagation of action potential activity in a predefined microtunnel neural network. *J. Neural Eng.*, **8**, 046031.

Raichman, N. & Ben-Jacob, E. (2008) Identifying repeating motifs in the activation of synchronized bursts in cultured neuronal networks. *J. Neurosci. Methods*, **170**, 96–110.

Rankov, V., Locke, R.J., Edens, R.J., Barber, P.R. & Vojnovic, B.. (2005) An algorithm for image stitching and blending. in Conchello, J.A., Cogswell, C.J. & Wilson, T.(Eds.), *Three-Dimensional and Multidimensional Microscopy: Image Acquisition and Processing XII*, Vol. **5701**, SPIE–International Society for Optics and Photonics, San Jose, CA, USA, pp. 190–199.

Rockland, K.S. (1998) Complex microstructures of sensory cortical connections. *Curr. Opin. Neurobiol.*, **8**, 545–551.

Rutten, W.L., Ruardij, T.G., Marani, E. & Roelofsen, B.H. (2007) Neural networks on chemically patterned electrode arrays: towards a cultured probe. *Acta Neurochirurg.*, **97**, 547–554.

Schreiner, C.E., Read, H.L. & Sutter, M.L. (2000) Modular organization of frequency integration in primary auditory cortex. *Annu. Rev. Neurosci.*, **23**, 501–529.

Shahaf, G., Eytan, D., Gal, A., Kermany, E., Lyakhov, V., Zrenner, C. & Marom, S. (2008) Order-based representation in random networks of cortical neurons. *PLoS Comput. Biol.*, **4**, e1000228.

Shein, M., Greenbaum, A., Gabay, T., Sorkin, R., David-Pur, M., Ben-Jacob, E. & Hanein, Y. (2009) Engineered neuronal circuits shaped and interfaced with carbon nanotube microelectrode arrays. *Biomed. Microdevices*, **11**, 495–501.

Slovin, H., Arieli, A., Hildesheim, R. & Grinvald, A. (2002) Long-term voltage-sensitive dye imaging reveals cortical dynamics in behaving monkeys. *J. Neurophysiol.*, **88**, 3421–3438.

Sporns, O., Tononi, G. & Edelman, G.M. (2000) Theoretical neuroanatomy: relating anatomical and functional connectivity in graphs and cortical connection matrices. *Cereb. Cortex*, **10**, 127–141.

Thorpe, S.J. & Fabre-Thorpe, M. (2001) Neuroscience. Seeking categories in the brain. *Science*, **291**, 260–263.

Tononi, G. & Edelman, G.M. (1998) Consciousness and complexity. *Science*, **282**, 1846–1851.

Tsuriel, S., Geva, R., Zamorano, P., Dresbach, T., Boeckers, T., Gundelfinger, E.D., Garner, C.C. & Ziv, N.E. (2006) Local sharing as a predominant determinant of synaptic matrix molecular dynamics. *PLoS Biol.*, **4**, e271.

Vanrullen, R. (2007) The power of the feed-forward sweep. *Adv. Cogn. Psychol.*, **3**, 167–176.

Wheeler, B.C. & Brewer, G.J. (2010) Designing neural networks in culture: experiments are described for controlled growth, of nerve cells taken from rats, in predesigned geometrical patterns on laboratory culture dishes. *Proc. IEEE*, **98**, 398–406.

Yvon, C., Rubli, R. & Streit, J. (2005) Patterns of spontaneous activity in unstructured and minimally structured spinal networks in culture. *Exp. Brain Res. Exp. Hirnforschung*, **165**, 139–151.

Zeki, S. & Bartels, A. (1998) The autonomy of the visual systems and the modularity of conscious vision. *Phil. Trans. R. Soc. Lond.*, **353**, 1911–1914.

Ziv, N.E. & Smith, S.J. (1996) Evidence for a role of dendritic filopodia in synaptogenesis and spine formation. *Neuron*, **17**, 91–102.